bandwidths of the $TCNQ^{0.59-}$ and the $TTF^{0.59+}$ stacks are estimated to be 0.40 and 0.65 eV, respectively (see Table II).[11,30] Thus from eq 11, the $E_R/4$ value of TCNQ is expected to be smaller than 0.10 eV, which is substantially smaller than the corresponding value of TTF, 0.26 eV (see table II). That is, the $TTF^{0.59+}$ stack has a substantially stronger tendency for intramolecular structural localization than does the $TCNQ^{0.59-}$ stack.[30]

In contrast to TTF·TNCQ, the selenium analogue TSF·TCNQ does not exhibit a $4k_f$ CDW but only a $2k_f$ CDW.[4b,4e,32] This finding and our conclusion that the $TSF^{0.63+}$ stack prefers a mono-valence structure (see Table II) show that electrons are delocalized in the $TSF^{0.63+}$ as well as in the $TCNQ^{0.63-}$ stacks. The difference between the $TTF^{0.59+}$ and the $TSF^{0.63+}$ stacks in their preference for a mixed-valence structure stems largely from the difference in the intramolecular relaxation energies E_R of TTF and TSF. We note that a $4k_f$ CDW is also observed from the organic salts TMTTF·TCNQ and HMTTF·TCNQ,[4b] both of which contain sulfur-based donor molecules. So far, TMTSF·DMTCNQ is the only salt of a selenium-based donor that gives rise to a $4k_f$ CDW.[4b,7c] Table I reveals that, among the selenium-based donors, TMTSF has the largest $E_R/4$ values, which is close in magnitude to that of a sulfur-based donor TMTTF or HMTTF. To determine whether the $4k_f$ CDW's in those salts are due to intramolecular structural localization or electronic localization, it would be necessary to carry out XPS studies on them.

Concluding Remarks

In this work it was shown necessary to take into consideration both electronic and intramolecular structural localizations in understanding the properties of organic conducting salts. Intramolecular structural localization leads to a mixed-valence structure and hence to electron localization (i.e., formation of unpaired electrons) in the absence of strong electron correlation. Consequently, intramolecular structural localization provides a mechanism to form a $4k_f$ CDW within the small-U limit. A number of experimental observations associated with organic salts that exhibit $4k_f$ CDW's seem better described by intramolecular structural localization than by electronic localization. From the viewpoint of solid-state physics, intramolecular structural localization arises from strong electron–optical phonon (or exciton) coupling on one molecular species.[7a,33]

The intramolecular structural localization condition, $E_R/4|\beta| > 1$, derived in the present work is isomorphic to the electronic localization condition, $U/4|\beta| > 1$. Intramolecular structural localization of a molecular stack arises when the intramolecular relaxation energy E_R of the stacking molecule is large compared with $4|\beta|$. For a donor molecule, the magnitude of E_R seems to be governed by its HOMO character: An increase in the antibonding character of the HOMO leads to an increase in E_R. Given a sulfur-based donor and its selenium analogue, the former has more antibonding character. This explains why sulfur-based donors are more likely to cause intramolecular structural localization and thus a $4k_f$ CDW than are selenium-based donors. This difference between sulfur- and selenium-based donors is eventually related to the fact that selenium has a greater size and polarizability than does sulfur.[7h] Thus, both the intramolecular structural and the electronic localization conditions are less favorable for molecular stacks of selenium-based donors. Clearly, an important strategy for eliminating electron localization in molecular stacks is to select stacking molecules of small E_R value. It is noted that both TMTSF and BEDT·TTF, which form the ambient-pressure superconductors $(TMTSF)_2ClO_4$[34] and β-$(BEDT\cdot TTF)_2X$ ($X^- = I_3^-$, IBr_2^-),[35] respectively, have small E_R values (see Table I).

To exemplify the electronic and structural localizations in organic conducting salts, we have examined the band electronic structures calculated for the mono-valence and mixed-valence structures of $TTF^{1/2+}$ and $TTF^{2/3+}$ stacks. This examination led us to formulate simple structural models of $2k_f$ and $4k_f$ distortions. Either in a mono-valence or in a mixed-valence stack, electron localization is essential for the occurrence of a $4k_f$ distortion.

Acknowledgment. This work was in part supported by the Camille and Henry Dreyfus Foundation through a Teacher-Scholar Award to M.-H. W., who thanks Dr. J. P. Pouget and Dr. C. Noguera for invaluable discussions and references. S.S.S. thanks Dr. Joel Bernstein and the Organic-Metals Group at Ben-Gurion University as well as Dr. E. Canadell, Dr. O. Eisenstein, and Dr. C. Minot for stimulating discussions.

Registry No. TTF, 31366-25-3; TMTTF, 50708-37-7; HMTTF, 57512-84-2; BEDT-TTF, 66946-48-3; TTF·TCNQ, 87952-99-6; TSF·TCNQ, 100840-36-6; $(TMTSF)_2PF_6$, 73261-24-2.

Contribution from the Department of Chemistry, Michigan State University, East Lansing, Michigan 48824, AT&T Bell Laboratories, Murray Hill, New Jersey 07974, and Department of Chemistry, University of Virginia, Charlottesville, Virginia 22901

Extended X-ray Absorption Fine Structure and Powder X-ray Diffraction Study of FeOCl Intercalated with Tetrathiafulvalene and Related Molecules

S. M. Kauzlarich,[†] B. K. Teo,*[‡] and B. A. Averill*[§]

Received July 30, 1985

For FeOCl and its intercalates, $FeOCl(TTF)_{1/8.5}$ (TTF = tetrathiafulvalene), $FeOCl(TMTTF)_{1/13}$ (TMTTF = tetramethylTTF), $FeOCl(TTN)_{1/9}(toluene)_{1/23}$ (TTN = tetrathianaphthalene), and $FeOCl(TTT)_{1/9}(toluene)_{1/24}$ (TTT = tetrathiatetracene), the combination of powder X-ray diffraction data and Fe K-edge EXAFS (extended X-ray absorption fine structure) spectroscopy provides a consistent picture of the structural changes of the FeOCl host upon intercalation. On the basis of these results and the analysis of neutron diffraction data, a structural model is proposed in which the intercalant TTF is parallel to the b axis (interlayer axis) and the central C=C bond is aligned with the c axis of FeOCl. TTN and TTT are also oriented parallel to the b axis, additionally tilted at an angle $\phi \cong 30°$ (ϕ is the angle between the ac plane and the S–S bond) to accommodate the short intramolecular S–S distance of 2.10 Å. TMTTF is oriented perpendicular to the b axis.

Introduction

Structural constraints are crucial in determining the properties of low-dimensional conductors.[1-3] Compounds known as organic metals beautifully illustrate this point. This category of compounds is composed of electron donor and acceptor molecules, which when crystallized as segregated stacks are generally conductors[4,5] (σ_{RT}

[†] Michigan State University. Current address: Department of Chemistry, Iowa State University, Ames, IA 50011.
[‡] AT&T Bell Laboratories.
[§] University of Virginia.

(1) "Physics and Chemistry of Low-Dimensional Solids"; Alcacêr, L., Ed.; D. Reidel: Dordrecht, Holland, 1980.
(2) Miller, J. S.; Epstein, A. J. *Prog. Inorg. Chem.* **1976**, *20*, 1-151.
(3) Hoffman, B. M.; Ibers, J. A. *Acc. Chem. Res.* **1983**, *16*, 15-21.
(4) Green, R. L.; Street, G. B. *Science (Washington, D.C.)* **1984**, *226*, 651-656.

0020-1669/86/1325-1209$01.50/0

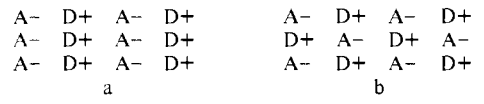

Figure 1. (a) Segregated stacks. (b) Mixed stacks of electron donors and acceptors.

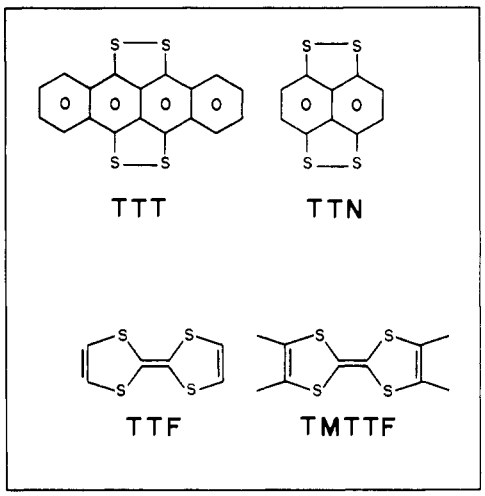

Figure 2. Schematic drawings of the organosulfur molecules intercalated into FeOCl.

$\cong$ 1000 $\Omega^{-1}cm^{-1}$) and when formed as mixed stacks are insulators[6] (see Figure 1). Thus, the electrical conductivity of the organic metals such as TTF–TCNQ (TTF = tetrathiafulvalene, TCNQ = tetracyanoquinodimethane) is due to the presence of segregated stacks of donors (TTF) and acceptors (TCNQ) and to the occurrence of partial charge transfer between the two.[7] Interest in organic metals has resulted in the synthesis of many new compounds, including salts containing inorganic anions (e.g. $(TMTSF)_2ClO_4$, and $[BEDT]I_3$, which are superconducting at ambient pressure at 1.4 and 1.3 K, respectively).[8,9] The fragility of these crystals as well as difficulties in synthesis has limited their applications to date. We have intercalated organic electron donors such as TTF into the inorganic material FeOCl.[10] A synthetic strategy of this type has the potential of obtaining new anisotropic materials with interesting properties if the host enforces a segregated stack structure upon the intercalant.

New phases prepared to date include $FeOCl(TTF)_{1/8.5}$, $FeOCl(TTF)_{1/9}(tol)_{1/21}$ (tol = toluene), $FeOCl(TMTTF)_{1/13}$, $FeOCl(TTN)_{1/9}(tol)_{1/23}$, and $FeOCl(TTT)_{1/9}(tol)_{1/24}$.[11,12] The structures of the planar organosulfur molecules are illustrated in Figure 2. These intercalation reactions occur with charge transfer from the guest to the host lattice and result in a ca. 10^3–10^4 increase in electrical conductivity over that of pristine FeOCl (σ_{RT} = 10^{-7} Ω^{-1} cm^{-1}, pressed powder). A number of structural studies have been performed on intercalated materials to aid in understanding the chemistry of such systems.[13,14] A combination of EXAFS spectroscopy, to probe the local Fe environment, and X-ray (this work) and neutron[15] powder diffraction, to probe the long-range ordering, has provided sufficient evidence for a consistent model for the orientation of those organosulfur molecules within FeOCl.

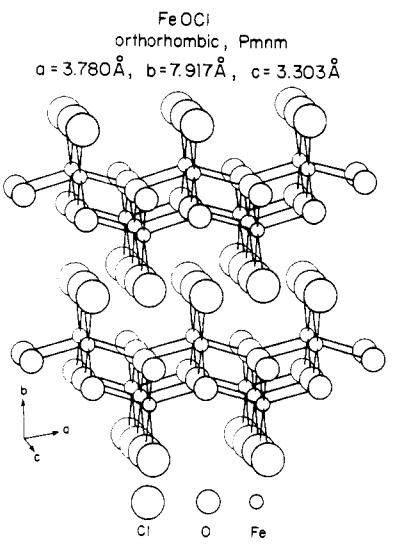

Figure 3. View of two layers of the FeOCl structure (adapted from ref 22).

Experimental Section

FeOCl was prepared by the usual sealed-tube technique.[16] X-ray powder diffraction and elemental analysis (Fe, Cl) were used to assess the integrity of the purple microcrystalline material. The intercalates were prepared by heating a solution of the organosulfur molecule with FeOCl (1:2 mole ratio) at a constant temperature (55–70 °C depending on intercalate) for 1–8 weeks. The black microcrystalline intercalates were subjected to X-ray powder diffraction and elemental analysis to assess completeness of intercalation and to determine composition. Mass spectrometry was used to provide information on co-intercalation by solvent. All manipulations were performed under inert atmosphere. X-ray diffraction data were recorded on a Huber Model 621 powder camera by asymmetric transmission using Cu $K\alpha_1$ radiation and silicon as an internal standard at the University of Virginia, Materials Science Department X-ray Laboratory. Lattice parameters were verified by using an X-ray program based on the relationship of spacing to reciprocal cell edges.[17]

EXAFS (extended X-ray absorption fine structure) and XANES (X-ray absorption near edge structure) spectra were obtained at CHESS (Cornell High-Energy Synchrotron Source) at experimental stations C-1 and C-2.[18] Spectra were obtained on four different occasions on the same and different sample preparations to ensure reproducibility. The samples were diluted with boron nitride in a glovebag under nitrogen atmosphere, pressed into homogeneous pellets in aluminum cells (3 × 19 mm), and sealed with 1-mil Kapton tape. The sample concentration was adjusted to obtain a value of $\mu x \cong 1$ in order to minimize thickness effects.[19] All spectra were taken with a beam width of 15 mm and a resolution of 1–2 eV. The monochromator was detuned by 50% to avoid contributions from higher harmonics. The spectra of the compounds were measured in transmission mode, where the incident and transmitted beam intensities were measured by ionization chambers of 8 and 30 cm in length, respectively, filled with nitrogen (flow type). The spectra were analyzed at Bell Laboratories, Murray Hill, NJ, by using programs described elsewhere[20] and adapted to run on a DEC PDP Model 11/45 minicomputer.

(5) Lyuovskaya, R. N. *Russ. Chem. Rev.* (*Engl. Transl.*) **1983**, *52*, 736–750.
(6) Khidekel, M. L.; Zhilyaeva, E. I. *Synth. Met.* **1981**, *4*, 1–34.
(7) Bechgaard, K.; Andersen, J. R. In "Physics and Chemistry of Low-Dimensional Solids", Alacacér, L., Ed.; D. Reidel: Dordrecht, Holland, 1980; pp 247–263.
(8) Bechgaard, K.; Carneiro, K.; Olsen, M.; Rasmussen, F. B.; Jacobsen, C. S. *Phys. Rev. Lett.* **1981**, *46*, 852–855.
(9) Williams, J. M.; Emge, T. J.; Wang, H. H.; Carlson, K. D.; Crabtree, G. W. *Inorg. Chem.* **1984**, *23*, 2558–2560.
(10) Antonio, M. R.; Averill, B. A. *J. Chem. Soc., Chem. Commun.* **1981**, 382–383.
(11) Averill, B. A.; Kauzlarich, S. M.; Antonio, M. R. *J. Phys.* (*Les Ulis, Fr.*) **1983**, *44*, C-1373–C-1376.
(12) Averill, B. A.; Kauzlarich, S. M. *Mol. Cryst. Liq. Cryst.* **1984**, *107*, 55–64.
(13) Whittingham, M. S., Jacobson, A. J., Eds. "Intercalation Chemistry"; Academic Press: New York, 1982.
(14) Levy, F., Ed. "Intercalated Layered Materials"; D. Reidel: Dordrecht, Holland, 1979.
(15) Kauzlarich, S. M.; Stanton, J. L.; Faber, J., Jr.; Averill, B. A., submitted for publication.
(16) Schafer, H. *Z. Anorg. Allg. Chem.* **1949**, *260*, 279–294.
(17) "The Powder Method in X-ray Crystallography", Azaroff, L. V.; Buerger, M. J. McGraw-Hill, New York, 1958, 46–55. Program written by D. Holtman, University of Virginia.
(18) Stations C-1 and C-2 use Si(111) and Si(220) monochromators, respectively. The Fe K-edge data obtained on both were identical, except for variations in noise.
(19) Stern, E. A.; Kim, K. *Phys. Rev. B: Condens. Matter* **1981**, *23*, 3781–3787.
(20) Antonio, M. R.; Teo, B. K.; Averill, B. A. *J. Am. Chem. Soc.* **1985**, *107*, 3583–3590.

Table I. Calculated and Observed X-ray Powder Diffraction Data for FeOCl[a]

I[b]	d_{obsd}[c]	h k l	d_{calcd}[c]
s	7.9158	0 1 0	7.9170
s	3.4093	1 1 0	3.4111
m	2.5364	0 1 2	2.5361
m	2.3735	1 1 1	2.3729
m	2.1787	1 3 0	2.1638
w	1.9785	0 4 0	1.9792
m	1.8895	2 0 0	1.8900
w	1.8350	2 0 1	1.8383
w	1.8082	1 1 3	1.8100
w	1.6503	0 0 2	1.6515
m	1.6167	0 1 2	1.6167
vw	1.5482	1 4 1	1.5487
m	1.5132	2 2 1	1.5155
mw	1.4855	1 1 2	1.4865
w	1.3916	2 3 1	1.3932
m	1.2420	2 0 2	1.2436
vvw	1.0602	0 2 3	1.0607

a = 3.780 Å, b = 7.917 Å, c = 3.303 Å

[a] λ(Cu Kα$_1$) = 1.540 56 Å; silicon as internal standard. [b] Relative intensities. [c] d spacings in Å.

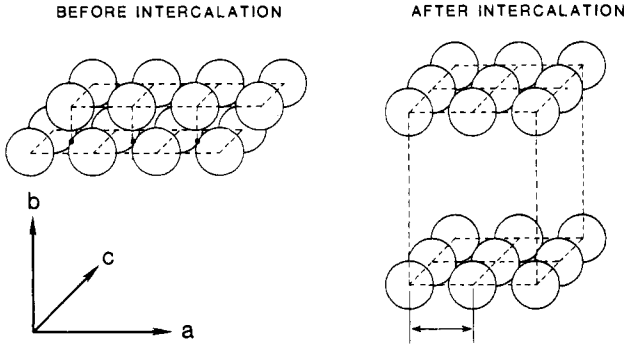

Figure 4. Illustration of the lateral shift of the chloride ion layers of FeOCl upon intercalation (adapted from ref 44).

X-ray Diffraction Results

The FeOCl structure consists of stacked neutral layers formed from distorted *cis*-$(FeCl_2O_4)^{7-}$ octahedra, which share half their edges to produce a central sheet of $(FeO)_n^{+}$ with Cl^- layers outermost on either side of the sheet.[21] The iron atoms share a single oxygen atom along the a axis and both a chloride and an oxygen atom along the c axis (Figure 3).[22] FeOCl crystallizes in an orthorhombic space group, *Pmnm*, with a = 3.780 Å, b = 7.917 Å, and c = 3.303 Å. These cell dimensions agree very well with the Bragg reflections observed in the X-ray powder diffraction (Table I).

Table II gives X-ray powder diffraction data for the tetrathiolene intercalates. The lattice parameters obtained from the X-ray powder diffraction data are given in Table III for FeOCl and the tetrathiolene intercalates. The data are consistent with expansion and doubling of the b axis, with alternate layers shifted one-half unit cell along the ac plane (Figure 4) giving rise to extinctions consistent with a body-centered unit cell of symmetry *Immm* or *I*222. This was originally proposed by Halbert and Scanlon[23] to describe the unit cell for FeOCl(metallocene)$_{1/x}$ and appears to be valid for the FeOCl(tetrathiolene)$_{1/x}$ intercalates as well. Early in this work, extinctions were not considered; it was thought that intercalation would decrease the number of observable X-ray peaks due to disorder of the lattice structure.[24,25] The decrease in the number of Bragg peaks of the intercalate compared to those of FeOCl can be attributed to the space group; body-centering increases the number of extinctions by including the requirement of $2n = h + k + l$.

TTT is the largest of the organosulfur molecules, and the TTT intercalate has the broadest X-ray peaks, suggesting that it is the least ordered of the intercalates. FeOCl(TTT)$_{1/9}$(tol)$_{1/24}$ may contain unintercalated FeOCl: a broad peak observed in the X-ray powder diffraction, centered at 8 Å, is always present. This peak at 8 Å can be attributed to either the (010) reflection of FeOCl (b = 7.917 Å) or to the (040) (b = 30.876) reflection of the intercalate. Very few reflections are observed for this compound, and only the b axis could be determined from the X-ray powder diffraction data. FeOCl(TMTTF)$_{1/13}$ shows the smallest expansion along the b axis, consistent with the intercalant oriented parallel to the layers.

Extended X-ray Absorption Fine Structure Results

The Fe K-edge transmission X-ray absorption and the $k^3\chi(k)$ spectra of FeOCl and the intercalates are shown in the supplementary material (Figures 1S–5S). The background absorption for all compounds was removed in k-space by using a cubic spline function of four sections (eq 1). The normalized oscillatory part

$$k = \left[\frac{2m}{\hbar^2}(E - E_0)\right]^{1/2} \quad (1)$$

of the absorption coefficient, in the form $k^3\chi(k)$, was obtained by dividing by the edge jump, $\Delta\mu_0$, and by correcting for $\mu(k)$ falloff with Victoreen's true absorption coefficient equation.[26,27] The edge jump, used to normalize the data, was taken as the step in the absorption coefficient at the K absorption edge. For all these spectra, the edge position energy, E_0, was determined as the photon energy at half-height of the absorption edge jump plus 13 eV (7124 eV). This provided a Fourier transform in which the magnitude of the first peak was the largest. The edge energy, E_0, was treated as an adjustable parameter in the final curve fitting of the data. ΔE_0 is defined as the threshold energy difference and was refined for each of the scattering atoms j (eq 2). This

$$\Delta E_{0_j} = E_0^{\text{theor}} - E_0^{\text{exptl}} \quad (2)$$

allows for discrepancies between empirically chosen energy thresholds, E_0^{exptl}, and theoretical E_0's, E_0^{theor}.[28] In the analysis, it was found that the amplitude of the first peak is sensitive to the number of sections of the spline, due to the short Fe–O distances (Fe–O, r = 1.961, 2.097 Å).

A Fourier filtering technique was employed to isolate peaks due to the absorbing atom's near neighbors. The resulting Fourier-filtered EXAFS spectra were subsequently truncated at 3.0 and 13.0 Å^{-1} to minimize distortion.[29] The Fourier-filtered curves were fit by using the standard formulation shown in eq 3.

$$k^3\chi(k) = \sum_j B_j F_j(k_j)\, k_j^2[\exp(-2\sigma_j^2 k_j^2)][\sin(2k_j r_j + \phi_j(k_j))]/r_j^2 \quad (3)$$

A nonlinear least-squares program for iterative estimations of parameters was used to refine the scale factors (independent of the photoelectron wavevector, k_j) for the scattering atoms of the jth type B_j, at a distance of r_j from the absorber, and the root-mean-square relative displacement σ_j (Debye–Waller factors) along r_j. Theoretical backscattering amplitude $F_j(k_j)$ and phase $\phi_j(k_j)$ functions, calculated by Teo and Lee,[30] were used in the curve-fitting formulation. The scale factor, B_j, is related to the

(21) Lind, M. D. *Acta Crystallogr., Sect. B: Struct. Crystallogr. Cryst. Chem.* **1972**, *B26*, 1058–1062.
(22) Halbert, T. R. In "Intercalation Chemistry"; Whittingham, M. S., Jacobson, A. J., Eds.; Academic Press: New York, 1982; pp 375–403.
(23) Halbert, T. R.; Scanlon, J. C. *Mater. Res. Bull.* **1979**, *14*, 415–421.
(24) Eckert, H.; Herber, R. H. *J. Chem. Phys.* **1984**, *80*, 4526–4540.
(25) Kauzlarich, S. M.; Averill, B. A.; Teo, B. K. *Mol. Cryst. Liq. Cryst.* **1984**, *107*, 65–73.
(26) Victoreen, J. A. *J. Appl. Phys.* **1948**, *19*, 855–860.
(27) "International Tables for X-ray Crystallography"; Kynoch Press: Birmingham, England, 1962; Vol. III, 171–173.
(28) Lee, P. A.; Beni, G. *Phys. Rev.* **1977**, *1513*, 2862–2883.
(29) Lee, P. A.; Citrin, P. H.; Eisenberger, P.; Kincaid, B. M. *Rev. Mod. Phys.* **1981**, *53*, 769–806.
(30) Teo, B. K.; Lee, P. A. *J. Am. Chem. Soc.* **1979**, *101*, 2815–2832.

Table II. X-ray Powder Diffraction Data for the Intercalates Showing the Calculated and Observed *d* Spacings for the Cell Parameters Given

I[a]	d_{obsd}[b]	*h k l*	d_{calcd}[b]	I[a]	d_{obsd}[b]	*h k l*	d_{calcd}[b]
			$FeOCl(TTF)_{1/9}(tol)_{1/21}$				
s	13.1694	0 2 0	13.078	m	2.3365	1 4 1	2.3361
s	6.5378	0 4 0	6.5390	m	1.8960	2 0 0	1.8960
s	3.4776	1 3 0	3.4773	w	1.8757	2 2 0	1.8764
w	3.0770	1 5 0	3.0702	mw	1.8077	1 10 1	1.8077
m	2.7664	0 5 1	2.8077	w	1.6638	0 0 2	1.6638
vw	2.5021	1 0 1	2.5011	vw	1.6511	0 2 2	1.6505
m	2.4838	0 7 1	2.4850	vw	1.5085	2 7 1	1.5074
w	2.4549	1 2 1	2.4566	vw	1.2507	3 3 0	1.2509
			a = 3.792 Å, b = 26.1560 Å, c = 3.3276 Å				
			$FeOCl(TTF)_{1/8.5}$				
s	13.099	0 2 0	13.009	w	2.1880	0 9 1	2.1862
m	6.511	0 4 0	6.505	m	1.8937	2 0 0	1.8937
s	3.474	1 3 0	3.471	mw	1.8748	2 2 0	1.8740
m	3.065	1 5 0	3.062	mw	1.8048	1 10 1	1.8048
m	2.8212	0 5 1	2.8116	mw	1.6706	0 0 2	1.6706
s	2.4842	0 7 1	2.4849	w	1.6568	0 2 2	1.6570
w	2.4604	1 2 1	2.4603	vw	1.5699	2 5 1	1.5705
m	2.3419	1 4 1	2.3381	m	1.5056	1 3 2	1.5053
			a = 3.7874 Å, b = 26.0193 Å, c = 3.3412 Å				
			$FeOCl(TMTTF)_{1/13}$				
s	11.588	0 2 0	11.672	w	1.6421	0 2 2	1.6422
m	5.834	0 4 0	5.836	w	1.5514	2 5 1	1.5504
m	3.394	1 3 0	3.4034	vw	1.5288	1 12 1	1.5341
s	2.7082	0 5 1	2.7043	mw	1.5082	1 3 2	1.4910
m	2.3586	0 7 1	2.3519	vw	1.4758	2 7 1	1.4742
vvw	2.0457	0 9 1	2.0434	vw	1.4711	2 10 0	1.4698
m	1.8923	2 0 0	1.8923	mw	1.2478	3 3 0	1.2453
mw	1.8679	2 2 0	1.8679	mw	1.2406	2 2 2	1.2403
m	1.6587	0 0 2	1.6587				
			a = 3.7846 Å, b = 23.3444 Å, c = 3.3174 Å				
			$FeOCl(TTN)_{1/9}(tol)_{1/23}$				
s	15.479	0 2 0	15.443	w	2.2501	1 6 1	2.2513
m	7.7014	0 4 0	7.722	w	2.1449	0 11 1	2.1474
m	3.5559	1 3 0	3.5583	m	1.8958	2 0 0	1.8960
w	3.2338	1 5 0	3.2317	m	1.8858	2 2 0	1.8819
w	2.9300	0 5 1	2.9332	m	1.8085	1 12 1	1.7945
w	2.6595	0 7 1	2.6595	m	1.5019	1 3 2	1.5091
w	2.3903	0 9 1	2.3909	mw	1.4841	2 9 1	1.4856
			a = 3.7920 Å, b = 30.8860 Å, c = 3.3329 Å				

[a] Relative intensities. [b] *d* spacings in Å.

Table III. Lattice Cell Parameters for FeOCl and $FeOCl(tetrathiolene)_{1/x}$ Obtained from X-ray Powder Diffraction (Cu $K\alpha_1$)

compd	*a*, Å	*b*, Å	*c*, Å
FeOCl	3.780	7.917	3.303
$FeOCl(TTF)_{1/9}(tol)_{1/21}$	3.792	26.156	3.328
$FeOCl(TTF)_{1/8.5}$[a]	3.787	26.019	3.341
$FeOCl(TMTTF)_{1/13}$	3.785	23.344	3.317
$FeOCl(TTN)_{1/9}(tol)_{1/23}$	3.782	30.886	3.332
$FeOCl(TTT)_{1/9}(tol)_{1/24}$	3.80[b]	30.876	3.34[b]

[a] No solvent included. [b] From EXAFS data.

number of nearest neighbors, N_j, of the jth type of atom and to the amplitude reduction factor, S_j, as follows in eq 4. The

$$B_j = N_j S_j \tag{4}$$

amplitude reduction factors, S_j, combine into one parameter many effects, including many-body effects, the energy resolution of the monochromator,[31] and thickness effects.[19,32]

The Fourier transforms of FeOCl, $FeOCl(TTF)_{1/8.5}$, and $FeOCl(TMTTF)_{1/13}$ are shown in Figure 5, while the Fourier transforms of FeOCl and $FeOCl(TTN)_{1/9}(tol)_{1/23}$ are compared directly in Figure 6. The first five peaks of the Fourier transforms are assigned as follows: Fe–O; Fe–Cl; Fe--Fe (nearest neighbors); Fe–Fe (*c* axis); Fe--Fe (*a* axis). From the comparison of the Fourier transforms of the FeOCl and $FeOCl(TTN)_{1/9}(tol)_{1/23}$ data, it is apparent that the FeOCl lattice is largely unperturbed upon intercalation (Figure 6). The first two peaks, due to Fe–O and Fe–Cl distances, were filtered by using a window of r' = 0.9–2.9 Å and fit by using Fe–O and Fe–Cl phase and amplitude functions. The next two partially resolved peaks (Fe--Fe nearest-neighbor and Fe--Fe *c* axis interactions) were filtered, r' = 2.0–3.6 Å, and fit with two terms by using Fe phase and amplitude functions while the Debye–Waller factors were held equal. The fifth peak, assigned to Fe--Fe (*a* axis) was filtered, r' = 3.2–3.8 Å, and fit by using one term. Multiple scattering was not a problem for Fe--Fe *c*-axis interactions due to the small Fe–O–Fe and Fe–Cl–Fe angles (104 and 88°, respectively). The Fe–O–Fe angle along the *a* axis is 149°, and the effects of multiple scattering are negligible.[33,34]

The best-fit parameters based on theoretical functions (BFBT) obtained from the curve fitting were adjusted by using the fine adjustment based on models (FABM) procedure outlined in the literature.[35-37] Pristine FeOCl was used as the model compound

(31) Lengeler, B.; Eisenberger, P. *Phys. Rev. B: Condens. Matter* **1980**, *21*, 4507–4520.
(32) Goulon, J.; Ginet-Goulon, C.; Cortes, R.; Dubois, J. M. *J. Phys. (Les Ulis, Fr.)* **1982**, *43*, 539–548.
(33) Teo, B. K. *J. Am. Chem. Soc.* **1981**, *103*, 3990–4001.
(34) Biebesheimer, V. A.; Marques, E. C.; Sandstrom, D. R.; Lytle, F. W.; Greegor, R. B. *J. Chem. Phys.* **1984**, *81*, 2599–2604.
(35) Teo, B. K.; Antonio, M. R.; Averill, B. A. *J. Am. Chem. Soc.* **1983**, *105*, 3751–3762.

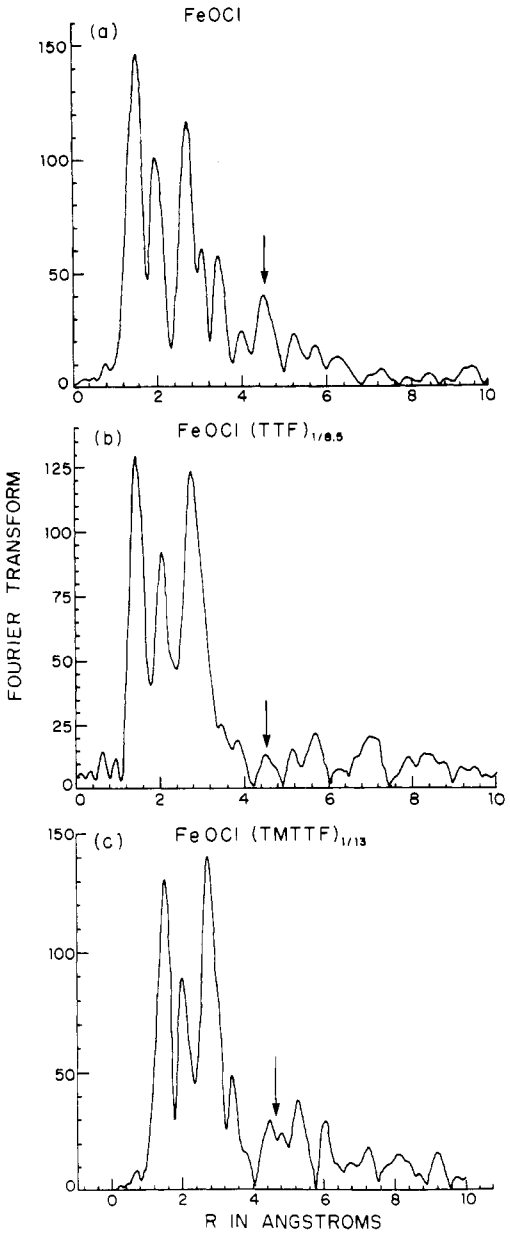

Figure 5. Fourier transforms of the Fe K-edge transmission EXAFS k^3 $\chi(k)$ vs. r: (a) FeOCl, (b) $FeOCl(TTF)_{1/8.5}$, (c) $FeOCl(TMTTF)_{1/13}$.

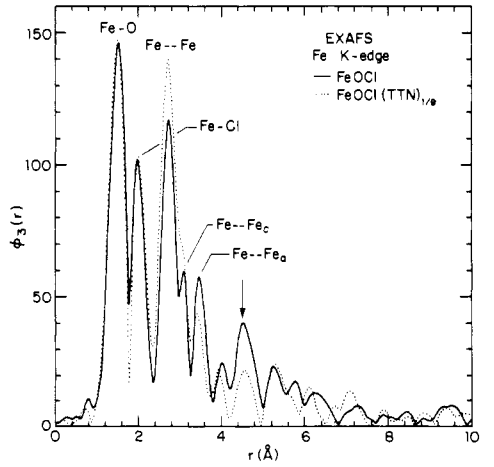

Figure 6. Comparison of the Fourier transforms of the Fe K-edge transmission EXAFS k^3 $\chi(k)$ vs. r for FeOCl (solid curve) and $FeOCl(TTN)_{1/9}(tol)_{1/24}$ (dotted curve) indicating the peak assignments.

for the intercalates. The EXAFS distances and coordination numbers obtained by fine tuning the parameters resulting from the best fit to the data using theoretical functions are given in Table IV. Results for different preparations of FeOCl and $FeOCl(TTN)_{1/9}(tol)_{1/23}$ are shown in order to illustrate the reproducibility of the results. Notable trends in the data are (i) the Fe–Cl distances for the intercalate are consistently longer than those for the pristine material, (ii) Fe--Fe nonbonded distances are consistently shorter, and (iii) in all cases the c axis is elongated compared to that of FeOCl. The c axis has expanded about 1%, a significant amount for a well-defined extended lattice structure. Debye–Waller factors (σ) are given in Table V and are consistent with little or no disorder of the FeOCl intercalate lattice, in contrast to EXAFS results on MPS_3 intercalates.[38]

Discussion

In order to formulate a plausible structural model for the intercalates, it is necessary to consider the interactions between the chloride layer and the organosulfur molecule. Significant increases in Debye–Waller factors are observed for both the Fe–Cl and Fe–O bonds in the intercalates (Table V). The only exception is $FeOCl(TTF)_{1/8.5}$, for which σ(Fe–Cl) actually decreases; this material also has the largest σ(Fe–O). The general increase in σ for the Fe–Cl bond is consistent with an interaction between the chlorine atoms and the intercalant molecules. A similar increase in σ is observed for the Fe–O bonds but is more difficult to interpret because backscattering by low Z atoms such as O dominates the EXAFS at small k, where theory is least accurate. Nonetheless, the results are consistent with increased disorder of the lattice upon intercalation. Since intercalation of the tetrathiolene guests is known to occur with electron transfer to the host,[10-12] some changes in the structure of FeOCl are expected. The changes observed are relatively minor compared to those observed for, e.g., $MnPS_3$, where intercalation results in loss of Mn^{2+} from the host,[38] and indicate that the FeOCl host layers remain intact upon intercalation. The relatively strong peak observed at $r' = 4.6$ Å for FeOCl (indicated by arrows in Figures 5 and 6) is best assigned to an Fe--Cl interaction between Fe of one layer and the nearest chlorine atom in an *adjacent* layer[39] (crystallographic distance 4.9 Å[20]). Upon intercalation, this peak is greatly reduced in intensity, as indicated by the arrows in Figures 5 and 6. In the intercalates, the FeOCl layers are separated by the organic intercalants, and consequently each Fe "sees" a different atom (C, H, or S) at this distance. This is expected to decrease the intensity of the peak dramatically.

A model was proposed earlier,[25] based on the sulfur atoms of the intercalant and the chlorine atom of FeOCl interacting as hard spheres of fixed van der Waals radii. Careful evaluation of the present X-ray data, stimulated by the results of a recent independent neutron powder diffraction study,[15] leads to an alternative model in which the FeOCl layers are "locked" into place by the TTF molecules. As shown in Table II, doubling the b axis reduces the discrepancies between the observed and calculated d spacings of the mixed reflections. The ab plane of FeOCl is shown in Figure 7: with the chloride layers eclipsed, tilting of the TTF molecule cannot explain both the observed interlayer space and the relative orientation of the layers. The TTF molecule must therefore be oriented perpendicular to the FeOCl layers, as shown in Figure 7a, locking the layers in place. This forces the sulfur atoms of TTF to be ~3.15 Å from the chlorine atoms, well within the sum of the van der Waals radii (3.6 Å). If the sulfur atoms in TTF are considered to adopt sp^3 hybridization, repulsive interactions

(36) Antonio, M. R.; Teo, B. K.; Orme-Johnson, W. H.; Nelson, M. J.; Groh, S. E.; Lindahl, P. A.; Kauzlarich, S. M.; Averill, B. A. *J. Am. Chem. Soc.* **1982**, *104*, 4703-4705.

(37) Plots of the values obtained for ΔE vs. Δr and B vs. σ for FeOCl and the intercalates are supplied as supplementary material, where $\Delta r = r - r_{bf}$ (bf = best fit) and ΔE_0, B, and σ were defined in the text.

(38) (a) Michalowicz, A.; Clement, R. *Inorg. Chem.* **1982**, *21*, 3872-3877. (b) Clement, R. *J. Chem. Soc., Chem. Commun.* **1980**, 647-648.

(39) Other possible candidates include Fe--Fe and Fe--Cl interactions within a layer. The distance between Fe atoms located at $z = 1$ and $^1/_2$ is only 3.77 Å, while the shortest Fe--Cl nonbonded distance is 3.99 Å. The next nearest neighbor, based on the published crystal structure, is the Cl in an adjacent layer, at 4.9 Å.

Table IV. Distances (Å) and Coordination Numbers (CN) Obtained from the EXAFS Analysis for FeOCl and the Intercalates[a]

compd,[b] CN	Fe–O[c] (av 2.03 Å; CN = 4.0)	Fe–Cl[c] (av 2.368 Å; CN = 2.0)	Fe--Fe[c] (av 3.107 Å; CN = 4.0)	Fe--Fe_c[c] (av 3.302 Å; CN = 2.0)	Fe--Fe_a[c] (av 3.780 Å; CN = 2.0)
FeOCl	2.03 (2)	2.37 (5)	3.11 (2)	3.30 (2)	3.78 (2)
	4 (1)	2.0 (7)	4 (1)	2 (1)	2.0 (8)
FeOCl[d]	2.03 (4)	2.36 (5)	3.11 (2)	3.30 (2)	3.78 (1)
	4 (1)	2 (1)	4 (2)	2.0 (8)	2 (1)
TTF[e]	2.03 (4)	2.42 (5)	3.08 (1)	3.33 (1)	3.78 (4)
	3 (1)	2 (1)	4 (1)	3 (1)	1 (1)
TTF[f]	2.03 (3)	2.40 (3)	3.09 (2)	3.31 (2)	3.78 (2)
	4 (1)	2 (1)	4.5 (2)	2 (1)	2 (1)
TTN	2.04 (4)	2.41 (4)	3.08 (1)	3.34 (2)	3.80 (3)
	3.1 (6)	1.5 (9)	4 (1)	2 (1)	2.0 (5)
TTN[d]	2.03 (3)	2.40 (4)	3.08 (1)	3.35 (2)	3.77 (3)
	4 (2)	2 (1)	3.8 (6)	1.5 (5)	2 (1)
TTT	2.04 (4)	2.39 (5)	3.07 (1)	3.34 (2)	3.80 (2)
	3.8 (9)	1.5 (7)	3.3 (5)	1.3 (5)	1 (1)
TMTTF	2.03 (3)	2.38 (4)	3.08 (1)	3.32 (1)	3.80 (2)
	4 (1)	2 (1)	5 (1)	3 (2)	1.8 (3)

[a] First row of values for each compound are distances; second row, coordination numbers. [b] The intercalates are represented by the guest species. [c] Fe–X distances obtained from ref 21. [d] A different preparation to illustrate the reproducibility of the EXAFS analysis. [e] $FeOCl(TTF)_{1/8.5}$. [f] $FeOCl(TTF)_{1/9}(tol)_{1/21}$.

Table V. Debye–Waller Factors (Å) Obtained from the Best Fit to the Experimental Data Using Theoretical Functions

compd[a]	Fe–Cl[b]	Fe–O	Fe–Fe_c[b]	Fe–Fe_a[b]
FeOCl	0.069	0.035	0.069	0.074
TTF[c]	0.050	0.060	0.075	0.074
TTF[d]	0.072	0.040	0.088	0.095
TTN	0.100	0.041	0.073	0.068
TTT	0.078	0.045	0.063	0.061
TMTTF	0.092	0.047	0.075	0.059

[a] The intercalates are represented by the guest species. [b] Debye–Waller factors for these interactions are listed in Å. [c] $FeOCl(TTF)_{1/8.5}$. [d] $FeOCl(TTF)_{1/9}(tol)_{1/21}$.

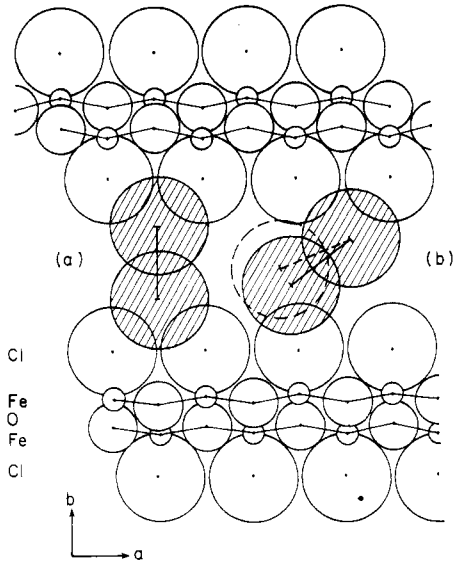

Figure 7. Schematic representation of the possible orientations of TTF. Shaded circles indicate the sulfur atoms of the intercalant.

between the lone-pair electrons on sulfur and the chlorine atoms of FeOCl will be minimized in this arrangement.

The distance between sulfur atoms in adjacent rings of TTF is 3.4 Å. If one sulfur atom occupies a hole formed by four chlorine ions of an FeOCl layer, then the sulfur on an adjacent ring must occupy the next hole along the *c* axis, due to the approximate match between the S---S distance and the repeat distance along *c* (3.3 vs. 3.8 Å along *a*). This results in alignment of the TTF molecules along the *c* axis (Figure 8). The observed elongation along *c* in the intercalates is thus viewed as resulting from a perturbation of the FeOCl lattice by the slightly larger S---S spacing within the TTF molecule. In addition, the Fourier

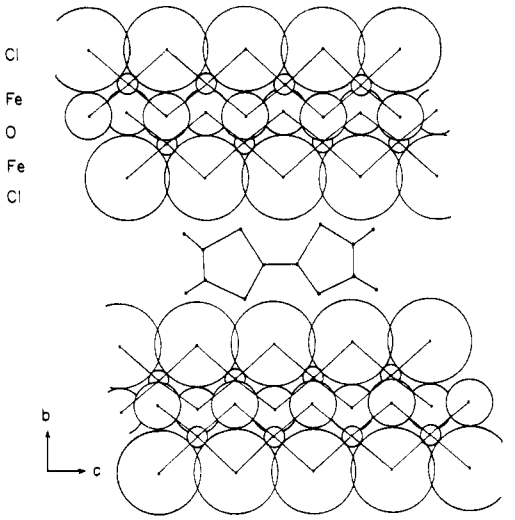

Figure 8. Schematic representation of the orientation of TTF, showing the approximate match between the S--S distance of TTF and the *c* axis repeat distance of the FeOCl host lattice.

transform of $FeOCl(TTF)_{1/8.5}$ shows a greatly decreased intensity for the peak assigned to the Fe--Fe interaction along *a* (Figure 5), such that the peak is not resolved. Inclusion of an Fe--Fe_a term in the curve fitting results in an improved fit, but the coordination number obtained is 1 ± 1. The reason for the reduced intensity of this peak relative to that of FeOCl or the other intercalates is not clear; it may be due to disorder induced in the FeOCl lattice by an irregular slipped-stack arrangement of TTF molecules along the *a* axis.

Both the X-ray powder data and the EXAFS data indicate that the intercalates (except for $FeOCl(TTT)_{1/9}(tol)_{1/24}$) are well-defined solids with essentially undistorted FeOCl layers. This supports the hypothesis that the layers are locked by the intercalant. Locking of the host layers by an intercalant has been noted previously for metallocenes intercalated into TaS_2.[40] The maximum stoichiometry predicted by this model is $FeOCl(TTF)_{1/8}$. The maximum experimental stoichiometry obtained to data is $FeOCl(TTF)_{1/8.5}$, in close agreement with the model, suggesting that the TTF molecules are approximately close-packed between the layers.

The TMTTF molecule in $FeOCl(TMTTF)_{1/13}$ must be oriented *parallel* to the FeOCl layers to account for the observed increase in interlayer spacing of only 3.7 Å, which is substantially less than

(40) Clement, R. P.; Davies, W. B.; Ford, K. A.; Green, M. L. H.; Jacobson, A. J. *Inorg. Chem.* **1978**, *17*, 2754–2758.

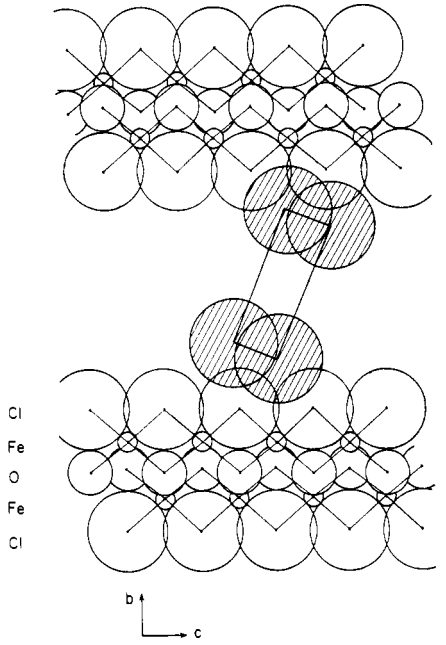

Figure 9. Schematic representation of the orientation of TTN and TTT taking into account the lateral shift of the FeOCl layers. Shaded circles indicate the sulfur atoms of the intercalant.

that observed for $FeOCl(TTF)_{1/8.5}$. (The van der Waals thickness of TMTTF is estimated to be 2.0 Å). This orientation is also consistent with the decreased stoichiometry observed for TMTTF vs. TTF. The electron density on sulfur, if considered to be located in sp^3 hybridized orbitals, again results in minimal interactions between the chlorine atoms and the sulfur atoms in the TMTTF molecule. Introduction of methyl groups has also been shown to result in a change in orientation of pyridine in TaS_2 from perpendicular to the layers to parallel to them.[41] Presumably the $-CH_3\cdots Cl(S)$ interactions are repulsive in nature and destabilize the perpendicular orientation in both systems.

The orientation of TTN and TTT is more difficult to determine. As in the hard-sphere model,[25] TTN and TTT must tilt at an angle ϕ (where ϕ is defined as the angle between the S–S bond and the *ac* plane) in order to accommodate the short (2.10 Å[42]) S–S bonded distance. Alignment of the molecule along the *c* axis will minimize sulfur–chlorine repulsive interactions and account for the observed interlayer distances if $\phi \cong 30°$, as shown in Figure 9.

Conclusion

X-ray powder diffraction data for all the intercalants can be adequately described by an orthorhombic cell with *a* unchanged, *c* increased about 1%, and *b* (the interlayer axis) expanded and doubled compared to the unit cell of pristine FeOCl. Comparison of the full widths at half-maximum of the X-ray powder diffraction peaks for the intercalates vs. FeOCl indicates that $FeOCl(TTT)_{1/9}(tol)_{1/24}$ is the least crystalline. The EXAFS data suggest that the FeOCl lattice remains rigid with little distortion of distances around the Fe upon intercalation. A model is proposed in which the tetrathiolene molecule is perpendicular to the FeOCl layers, thus locking the layers into an eclipsed conformation. The sulfurs on the TTF molecule are then closer to the chlorine atoms of FeOCl (3.15 Å) than the sum of the van der Waals radii (3.6 Å). Pseudotetrahedral (sp^3) hybridization is proposed for the electronic density on the sulfur atoms of TTF. Because of the short S–S bond of TTT and TTN, these intercalants must be tilted at an angle ϕ ($\sim 30°$) with respect to the FeOCl layers, with the molecule aligned along the *c* axis of FeOCl. The present data however, do not provide direct evidence for long-range ordering of the guest species. Further studies using solid-state NMR and inelastic neutron diffraction are under way to determine the extent of long- or short-range interactions of the guest species.

Acknowledgment. B.A.A. was an Alfred P. Sloan Foundation Fellow, 1981–1985. We thank O. Fussa, P. Lindahl, and A. Nagahisa for assistance with the collection of some of the EXAFS data. This research was supported by the National Science Foundation, Solid State Chemistry, Grant DMR-8542271 (B.A.A. and S.M.K.). We thank the staff at CHESS for their assistance.

Registry No. FeOCl, 13870-10-5; $FeOCl(TTF)_{1/8.5}$, 100858-11-5; $FeOCl(TMTTF)_{1/13}$, 100898-53-1; $FeOCl(TTN)_{1/9}(tol)_{1/22}$, 100858-12-6; $FeOCl(TTT)_{1/9}(tol)_{1/24}$, 100858-13-7; $FeOCl(TTF)_{1/9}(tol)_{1/23}$, 78829-78-4; $FeOCl(TTT)_{1/7}$, 87863-70-5.

Supplementary Material Available: Figures 1S–5S, raw data of Fe K-edge EXAFS of FeOCl and all intercalants,[43] Figure 6S, Fourier transforms of $FeOCl(TTT)_{1/7}$ and $FeOCl(py)_{1/3.6}$, and Figures 7S–9S, plots of ΔE_0 vs. Δr and *B* vs. σ used in the fine tuning of FeOCl and all intercalants (9 pages). Ordering information is given on any current masthead page.

(41) Kikkawa, S.; Kanamaru, F.; Koizumi, M. *Bull. Chem. Soc. Jpn.* **1979**, *52*, 963–966.
(42) Didebourg, O.; Toussaint, J. *Acta Crystallogr., Sect. B: Struct. Crystallogr. Cryst. Chem.* **1974**, *B30*, 2481–2485.
(43) Interested parties may obtain the raw data on tape upon request.
(44) Rouxel, J.; Palvadeau, P. *Rev. Chim. Miner.* **1982**, *19*, 317–332.